Science of the Total Environment 703 (2020) 135678

Contents lists available at ScienceDirect

Science of the Total Environment

journal homepage: www.elsevier.com/locate/scitotenv

High-efficiency As(III) oxidation and electrocoagulation removal using hematite with a charge—discharge technique

Lihu Liu [a,1], Hanchen Chen [a,1], Xiong Yang [a], Wenfeng Tan [a], Chengshuai Liu [b], Zhi Dang [c], Guohong Qiu [a,*]

[a] Key Laboratory of Arable Land Conservation (Middle and Lower Reaches of Yangtse River), Ministry of Agriculture and Rural Affairs, Hubei Key Laboratory of Soil Environment and Pollution Remediation, College of Resources and Environment, Huazhong Agricultural University, Wuhan 430070, China
[b] State Key Laboratory of Environmental Geochemistry, Institute of Geochemistry, Chinese Academy of Sciences, Guiyang 550081, China
[c] School of Environment and Energy, South China University of Technology, Guangzhou 510006, China

HIGHLIGHTS

- As(III) is oxidized and removed using hematite by multi-cycle charge—discharge.
- The highest removal ratio of As (T) reaches 98.6% at initial pH 7.0.
- ClO^- and the counter electrode contribute much to As(III) oxidation.
- As(T) removal can be ascribed to As (V) adsorption and precipitation on ferrihydrite.
- Electrode passivation is alleviated by the periodic redox reactions of electrode.

GRAPHICAL ABSTRACT

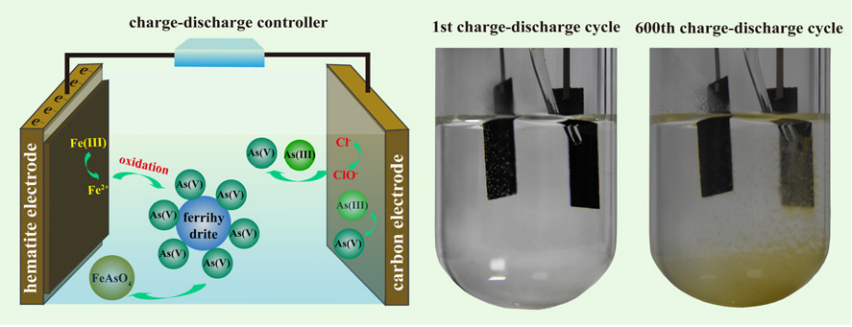

ARTICLE INFO

Article history:
Received 26 September 2019
Received in revised form 15 November 2019
Accepted 19 November 2019
Available online 21 November 2019

Editor: Yifeng Zhang

Keywords:
Arsenic
Hematite
Electrochemical removal
Redox
Electrocoagulation
$FeAsO_4$

ABSTRACT

Arsenite (As(III)) is generally removed by adsorption or coprecipitation after being oxidized to arsenate (As(V)). Electrocoagulation is regarded as an effective and environment-friendly method for arsenic (As) removal from wastewater. However, some disadvantages including the passivation of electrode and high energy consumption limit its wide application. Herein, a multi-cycle galvanostatic charge—discharge technique was employed to remove aqueous As(III) using hematite prepared through a microwave-assisted hydrothermal reaction. When charge—discharge experiments were conducted at the potential window of −0.8–0 V (*vs.* SCE) in As(III) solution with NaCl as the background electrolyte, ClO^- intermediates and the counter electrode at high potential contributed much to As(III) oxidation. As(V) was adsorbed on ferrihydrite generated from the re-oxidation of released Fe^{2+}, forming $FeAsO_4$ precipitate. A higher removal ratio of As(T) was achieved at initial pH 7.0 compared with that at initial pH 5.0 and 9.0. When the hematite mass was 4, 10 and 15 mg, the removal ratio of As(T) reached 55.2%, 79.6% and 98.6% after 600 cycles of charge—discharge. The periodic redox reactions of hematite electrodes occurred in each charge—discharge process, effectively avoiding the passivation of electrode. Additionally, the electrochemical system can be used as a supercapacitor for power output. The present work provides a novel strategy for high-efficiency As(III) immobilization and removal from aqueous solution.

* Corresponding author.
E-mail address: qiugh@mail.hzau.edu.cn (G. Qiu).
[1] Liu L.H. and Chen H.C. contributed equally to this work and shared the first author.

https://doi.org/10.1016/j.scitotenv.2019.135678
0048-9697/

1. Introduction

The excess intake of toxic metalloid As leads to diseases of skin, liver, kidney and other organs, and even cancers in human bodies (Bindal and Singh, 2019; Choong et al., 2007). The permissible limit set by the World Health Organization for As concentration is 0.01 mg L^{-1} in drinking water (Sorg et al., 2014). Geological causes and uncontrolled industrial activities are the main sources of As contamination in waters (Nordstrom, 2002; Qiao et al., 2018; Shakoor et al., 2019). It has been reported that As existing in groundwaters is posing threat to around 100 million people in India (Bindal and Singh, 2019). The average As concentration was about 10 mg L^{-1} in the wastewater discharged from the gold mine industry of Ghana (Fox et al., 2016). In Saskatchewan, Canada, the highest concentration of As reached 71 mg L^{-1} in the waters obtained from uranium mine mill tailings (Donahue and Hendry, 2003; Wang and Mulligan, 2006). Therefore, it is urgent to develop some high-efficiency and low-cost techniques for As removal from aqueous solution.

The toxicity of As varies with species. At neutral pH, As(III) and As(V) mainly exist in the forms of H_3AsO_3 and $H_2AsO_4^-$/$HAsO_4^{2-}$, respectively, and As(III) shows higher mobility and toxicity than As(V) (Sorg et al., 2014). As(III) is generally removed by adsorption or coprecipitation after being oxidized to arsenate As(V) during the treatment of As(III)-containing wastewater (Gude et al., 2017; Nidheesh and Singh, 2017). The rich iron (hydr)oxides in nature, including ferrihydrite, goethite and hematite, have high affinity for As (Luong et al., 2018; Park et al., 2016). For example, As(V) can be adsorbed on ferrihydrite surface, forming a complex or amorphous $FeAsO_4$ (Luong et al., 2018). Therefore, these iron (hydr)oxides are widely used for As(V) removal.

Recently, electrochemical technologies have been extensively developed and applied in As removal owing to its environmental friendliness and high efficiency (Dai et al., 2017; Nidheesh and Singh, 2017). Electrocoagulation has the advantages of easy operation and high efficiency compared with the traditional chemical coagulation and precipitation (Song et al., 2017). Currently, elemental Fe is the main iron-based material used for As electrocoagulation. In the electrocoagulation for As, Fe anode is sacrificially oxidized to Fe^{2+} and subsequently released into the solution. As(V) adsorption and coprecipitation lead to the formation of $FeAsO_4$ during the re-oxidation of released Fe^{2+} to amorphous iron (hydr)oxides, which facilitates the immobilization and removal of As (Song et al., 2017). However, some disadvantages including the passivation of electrode and high energy consumption largely hinder the wide application of traditional electrocoagulation (Holt et al., 2005; Song et al., 2017).

Cyclic redox of Fe(II) and Fe(III) occurs in iron oxide crystal when it is used as a supercapacitor electrode material (Nithya and Arul, 2016). Our previous studies have indicated that electrochemically-controlled redox reactions can significantly improve the adsorption performance of manganese oxides for heavy metal ions including Zn^{2+}, Cd^{2+}, and Cu^{2+} (Liu et al., 2017; Liu et al., 2019a; Peng et al., 2016; Yang et al., 2018). The dissolution−recrystallization of manganese oxides driven by electrochemical redox reactions was also found to contribute to As(III) oxidation and As(V) adsorption (Liu et al., 2019b). Fe^{2+} can be released to the solution during the electrochemical reduction of iron (III) oxides, which may affect the removal of contaminants including Cr and As. For example, the electrochemical reduction of magnetite to Fe^{2+} enhances Cr(VI) removal capacity *via* reduction of Cr(VI) to Cr$(OH)_3$ precipitate (Yang et al., 2019). In As(V)-containing solution, amorphous iron (hydr)oxides generated from Fe^{2+} oxidation can have precipitation reaction with As(V) (Khan et al., 2000). In addition, O_2 may be reduced to H_2O_2 on electrode surface (Wang et al., 2014). H_2O_2 and its secondary product OH• formed under the catalysis of Fe^{2+} facilitate As(III) oxidation (Wang et al., 2014). However, little is known about the As(III) removal by iron (hydr)oxides under electrochemically controlled redox reactions.

The electrochemical performance of electrode materials depends on the properties including particle size and micromorphology (Luo et al., 2016). Microwave-assisted hydrothermal method has the advantages of low cost and easy operation in the preparation of iron oxides with uniform and controllable particle size and morphology (Qiu et al., 2011). In this work, microwave-assisted hydrothermal reaction was employed to prepare nanosized hematite. The removal of As(III) using hematite electrode was performed by multi-cycle galvanostatic charge−discharge with different initial pH values and hematite mass. The pristine hematite and the solid intermediate products were characterized, and OH•, H_2O_2 and ClO^- were also quantitatively detected in the removal processes. The aims of this work are to clarify the electrochemical removal process and mechanism of As(III) by charge−discharge using hematite and provide a novel strategy for As removal from wastewaters.

2. Experimental section

2.1. Preparation of hematite

The microwave-assisted hydrothermal reaction for hematite synthesis was reported in our previous work (Qiu et al., 2011). The quartz tube with a mixed solution of 0.1 mol L^{-1} $Fe(NO_3)_3$ (10 mL) and 0.5 mol L^{-1} urea (10 mL) was transferred into a Discover SP microwave reactor (CEM Corporation). The reactor was temperature programmed to 120 °C and maintained for 20 min. After reaction, the precipitate was washed using pure water by centrifugation. The obtained solid was dried in a vacuum oven at 40 °C for 12 h.

2.2. Electrochemically controlled As(III) removal

As(III) removal was performed in a three-electrode system with a volume of 30 mL at room temperature in air atmosphere. The working electrode was prepared by coating a mixture of hematite, acetylene black and polyvinylidene fluoride with a mass ratio of 75:15:10 on a carbon fabric. Detailed preparation of the working electrode was described in our previous work (Liu et al., 2019a). The coated area of the working electrode was 1.5 cm × 2.5 cm, and the mass of hematite was controlled to be 4.0 mg on the electrode. Another blank carbon fabric and a saturated calomel electrode (SCE) were used as the counter and reference electrodes, respectively. As(III) solutions (100 mg L^{-1}) were prepared using $NaAsO_2$ with NaCl (10 mmol L^{-1}) as the background electrolyte. HCl or NaOH solutions (0.1–1.0 mol L^{-1}) were used to adjust the initial pH of the As(III)-containing NaCl solution to 7.0. Multi-cycle galvanostatic charge−discharge at the potential window of −0.8–0 V (*vs.* SCE) and a current density of 0.1 A g^{-1} was controlled by a battery testing system (Shenzhen Neware Electronic Co., Ltd., China). A CHI660E electrochemical workstation (Shanghai Chenhua Instrument Co., Ltd., China) was used to monitor the cell voltage.

The effect of initial pH (5.0, 7.0 and 9.0) on As(III) electrochemical removal was investigated. The hematite mass on the working electrode was increased to 10 and 15 mg, respectively, to evaluate the effect of hematite mass, and the size of the working electrode with different hematite mass was shown in Table S1. The isothermal adsorption of As(III) on hematite and the chemical coagulation of As(III) and As(V) by $Fe(NO_3)_3$ were conducted to further analyze the electrochemical removal mechanism. The detailed chemical coagulation conditions are shown in the Supporting Information (Supporting Methods).

2.3. Analytical methods

The crystal structure, chemical composition, micromorphology and crystal size of the solid products were respectively characterized

by power X-ray diffraction (XRD, Bruker D8 ADVANCE, Cu Kα, λ = 0.15406 nm), Fourier-transform infrared spectroscopy (FTIR, Bruker VERTEX 70), field emission scanning electron microscopy (FESEM, SU8000, Hitachi) and high-resolution transmission electron microscopy (HRTEM, FEI Talos F200C). A molybdenum blue method was used to analyze the concentrations of As(V) and As(T) (Dhar et al., 2004). As(III) concentration was calculated from the difference in the concentrations of As(V) and As(T). The concentrations of total dissolved Fe^{2+} and Fe^{3+} were analyzed using an atomic absorption spectroscope (Varian AA240FS). The determination of dissolved Fe^{2+} concentration was conducted using a 1,10-phenanthroline method on an UV-1800 ultraviolet–visible (UV–vis) spectrophotometer (Shanghai Mapada Instruments Co., Ltd., China) (Hong et al., 2018). A JPB-607A dissolved oxygen meter (Shanghai Precision and Scientific Instrument Co., Ltd., China) was used to monitor the concentration of dissolved oxygen. Benzoic acid (BA, 10 mmol L^{-1}) was used to quantitatively determine OH• formed in the electrochemical system with 4 mg hematite at initial pH 7.0 (Joo et al., 2005). A *N,N*-diethyl-*p*-phenylenediamine (DPD) method was used to analyze the concentrations of H_2O_2 and ClO^-, and peroxidase was used for H_2O_2 determination (Garg et al., 2016; Qiu et al., 2018). Peroxidase (10 mg L^{-1}) and higher concentration of NaCl (15 or 20 mmol L^{-1}) were respectively used to study the role of H_2O_2 and ClO^- in the electrochemical system with 4 mg hematite at initial pH 7.0. The As(T) and Fe contents in the working electrode after charge−discharge were analyzed by microwave digestion at 190 °C for 40 min using HCl and HNO_3 (volume ratio, 3:1). The charge−discharge processes were recorded using a camera. The As K-edge X-ray-absorption near-edge structure (XANES) spectra were collected on 1W1B beamline (Beijing Synchrotron Radiation Facility, China) in transmission mode to analyze the valence state of As in the working electrode after electrochemical removal. During the background removal, the E_0, *Rbkg* and k-weight were 11,867 eV, 1.1 Å, and 3, respectively. The references of $FeAsO_4$ and ferrihydrite were prepared by mixing the solutions of Na_3AsO_4 and $Fe(NO_3)_3$ and adding NaOH solution to a $Fe(NO_3)_3$ solution, respectively (Jiang et al., 2015; Jones et al., 2009).

3. Results

3.1. Hematite characterization

Fig. 1a and b show the XRD pattern and FTIR spectrum of the synthesized hematite. All diffraction peaks observed in the XRD pattern can be well indexed to the planes of hematite (JCPDS No. 89–0599). The bending and stretching vibrations of Fe−O occurred with absorption peaks at 573 and 457 cm^{-1} (Wang et al., 1998). The absorption bands at 1061 and 1345 cm^{-1} represent the residual O−H on hematite surface (Luo et al., 2016). The absorption bands at 1630 and 3398 cm^{-1} are due to the bending and stretching vibrations of water, respectively (Liu et al., 2018). Hematite with particle size of about 5 nm was observed in HRTEM image, and the interplanar spacing of 0.25 nm was in good agreement with the (110) plane (Fig. 1c and d).

3.2. As(III) removal performance of hematite

The electrochemical removal of As(III) was performed in a three-electrode system containing 4 mg hematite. In NaCl solution, the pH decreased from 7.0 to 4.9, and the dissolved Fe^{2+} concentration reached 3.2 mg L^{-1} after 600 cycles of charge−discharge. Fig. 2a shows the concentrations of different As species in As(III) solution (100 mg L^{-1}) at initial pH 7.0 in the charge−discharge processes. The concentration of As (III) and As(T) decreased, and that of As(V) increased first and then reached equilibrium with increasing cycle number, indicating the oxidation of a part of As(III). After 600 cycles, the concentrations of As (III), As(V) and As(T) were 15.3, 33.5 and 44.8 mg L^{-1}, respectively, and the corresponding As(T) removal ratio was 55.2% (Fig. S1). The As (T) removal capacity (414.0 mg g^{-1}) was significantly higher than that of isotherm adsorption (60.9 mg g^{-1}) (Fig. S2).

About 68.4% Fe was released to the solution from the working electrode after charge−discharge, as indicated by the chemical analysis. No Fe^{3+} was detected during As(III) removal in the solutions. With increasing cycle number, Fe^{2+} concentration increased first and reached the maximum (3.4 mg L^{-1}) after 200 cycles, and then decreased to 0.8 mg L^{-1} after 600 cycles (Fig. 2b). The change tendency of pH was

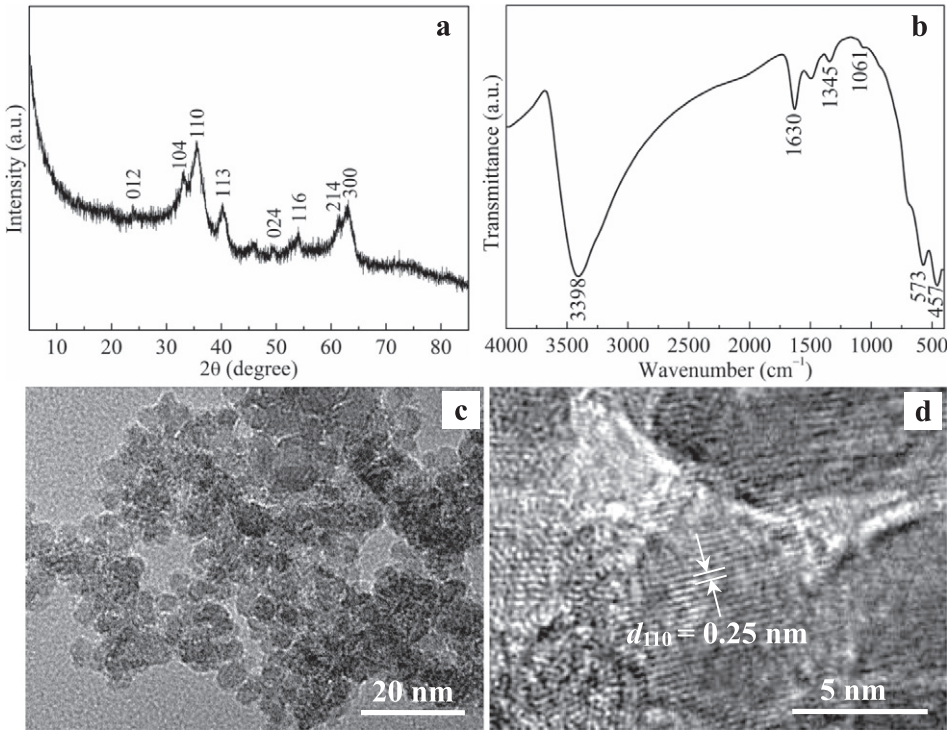

Fig. 1. XRD pattern (a), FTIR spectrum (b), HRTEM image (c) and the corresponding magnified image (d) of the as-prepared hematite.

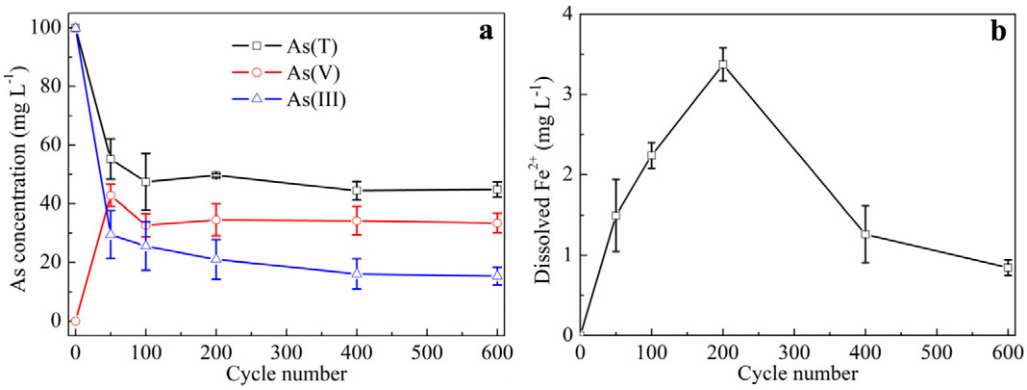

Fig. 2. Concentrations of As(III), As(V) and As(T) (a) and the corresponding dissolved Fe^{2+} concentration (b) in the mixed solution of 100 mg L^{-1} As(III) and 10 mmol L^{-1} NaCl at initial pH 7.0 after different cycles of charge−discharge of the working electrode with 4 mg hematite.

similar to that of Fe^{2+} concentration (Fig. S3). The pH rapidly decreased from 7.0 to 3.7 during the first 50 cycles, then decreased to 3.4 after 200 cycles, and finally increased to 4.2 after 600 cycles. No obvious difference was observed in dissolved oxygen concentrations in 10 mmol L^{-1} NaCl and As(III)-containing NaCl solutions (Fig. S4). Dissolved oxygen concentration decreased first and reached the minimum after 50 cycles, and then slightly increased with increasing cycle number. The potential of the counter electrode ranged from −0.8 to 1.9 V in the charge−discharge processes (Fig. S5).

The concentrations of accumulated OH•, instant H_2O_2 and ClO^- were quantitatively determined in the electrochemical removal system (Fig. 3). The concentration of accumulated OH• increased with increasing cycle number, and reached 38.3 μmol L^{-1} after 600 cycles. The instant concentration of H_2O_2 increased first and reached the maximum (1.59 μmol L^{-1}) after 400 cycles, and then decreased with increasing cycle number. The concentration of ClO^- increased first and reached the maximum (1.48 μmol L^{-1}) after 200 cycles, and then decreased with increasing cycle number.

The charge−discharge processes of the electrochemical system were recorded using a camera. Brown precipitate was observed at the bottom after 600 cycles of charge−discharge in NaCl solution (Fig. S6). In the presence of As(III), light yellow precipitate was formed and the amount increased with increasing cycle number (Fig. 4). The electrode and precipitate formed in the charge−discharge processes were collected and characterized using XRD, FTIR, XAS and SEM to analyze the As(III) removal mechanism.

Fig. S7a shows the XRD patterns of hematite electrodes after charge−discharge in 10 mmol L^{-1} NaCl and As(III)-containing NaCl solutions. The crystal structure of hematite changed little and no diffraction peak of other minerals was observed after the charge−discharge. In As(III)-containing NaCl solution, the diffraction intensity of (110) plane of hematite decreased with increasing cycle number. Fig. S7b shows the FTIR spectra of pristine hematite and hematite electrode after charge−discharge in As(III)-containing NaCl solution. The absorption peak at 829 cm^{-1} demonstrated the stretching vibration of As—O in amorphous $FeAsO_4$ (Hong et al., 2018; Jiang et al., 2015), indicating the adsorption of As on hematite electrode after charge−discharge in As(III)-containing NaCl solution. The results of chemical analysis showed that the As(T) content on hematite electrode accounted for 4.2% of the removed As(T) from the solution. The FESEM images indicated that some nanoparticles were formed on the hematite electrode after charge−discharge in NaCl solution, and the dissolution of hematite occurred after charge−discharge in As(III)-containing NaCl solution (Fig. S8).

Fig. 5a shows the XRD patterns of the precipitate formed in NaCl and As(III)-containing NaCl solutions after 600 cycles of charge−discharge. A mixture of ferrihydrite and lepidocrocite was formed in NaCl solution, while ferrihydrite and $FeAsO_4$ were the main products generated in As(III)-containing NaCl solution. The XANES was used to fit the valence state of As in the precipitate formed in As(III)-containing NaCl solution (Fig. 5b). In the linear combination fitting, the spectra of $NaAsO_2$ and $FeAsO_4$ were used as the references for As(III) and As(V), respectively. The fitting results showed that the relative content of As(III) and As(V) was 13.4% and 86.6%, respectively. The corresponding FTIR spectra of the precipitates indicated that a lepidocrocite and ferrihydrite mixture and amorphous $FeAsO_4$ were respectively formed in NaCl and As(III)-containing NaCl solutions (Fig. S9). FESEM images indicated that nanosheets and nanoparticles were formed in NaCl solution, and nanoparticles were formed in As(III)-containing NaCl solution (Fig. S10).

3.3. Effects of initial pH and hematite mass on As(III) removal

The As removal efficiency is strongly influenced by pH in electrocoagulation. Fig. 6 shows the concentrations of different As

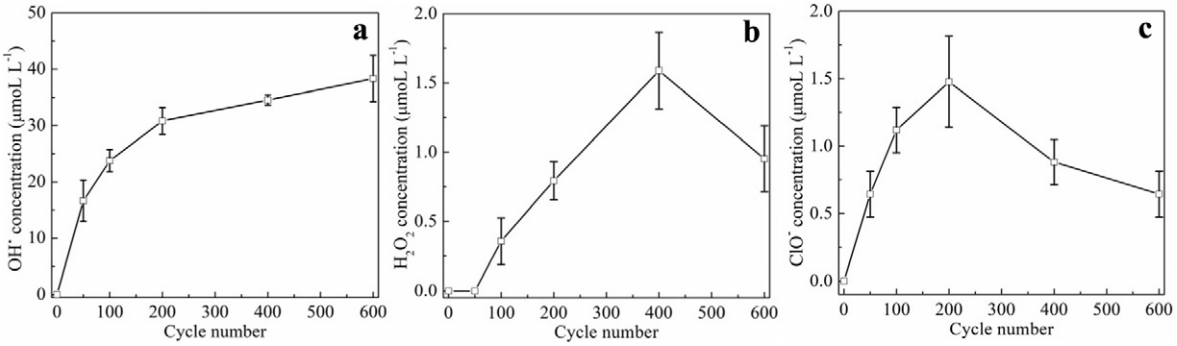

Fig. 3. Concentrations of accumulated OH• (a), instant H_2O_2 (b) and ClO^- (c) in the mixed solution of 100 mg L^{-1} As(III) and 10 mmol L^{-1} NaCl at initial pH 7.0 after different cycles of charge−discharge of the working electrode with 4 mg hematite.

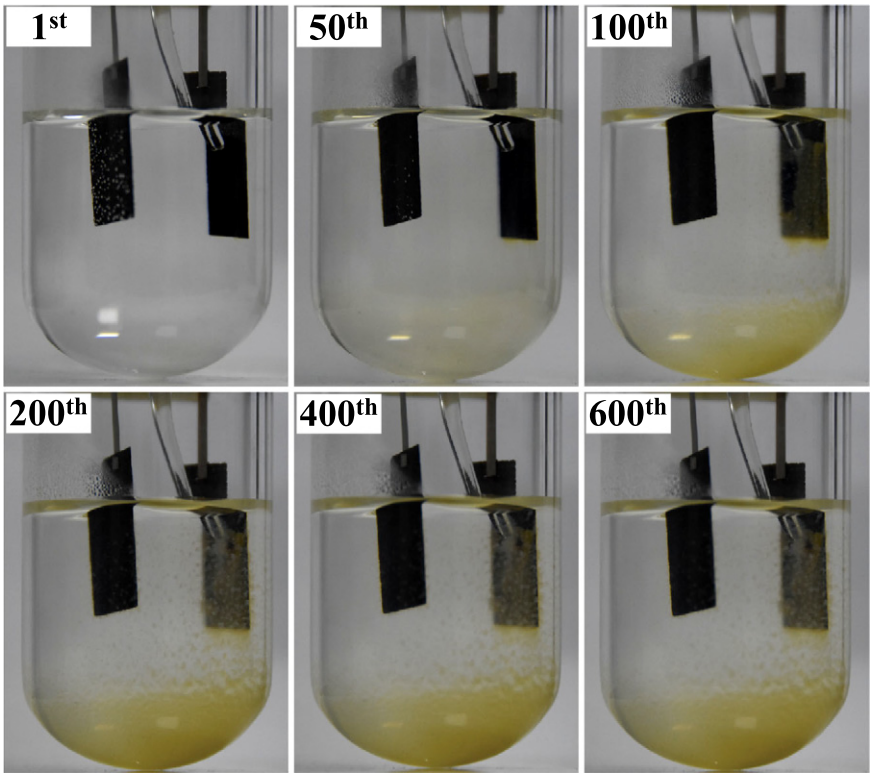

Fig. 4. Photographs of a three-electrode system with 4 mg hematite after 1, 50, 100, 200, 400 and 600 cycles of charge—discharge tests in the mixed solution of 100 mg L^{-1} As(III) and 10 mmol L^{-1} NaCl at initial pH 7.0 in air atmosphere. The left, middle and right electrode are counter, reference and working electrode, respectively.

species in As(III) solution (100 mg L^{-1}) at initial pH 5.0 and 9.0 during the charge—discharge processes of the working electrode containing 4 mg hematite. At initial pH 5.0 and 9.0, the concentration of As(III) and As(T) decreased, and that of As(V) increased with increasing cycle number. After 600 cycles of charge—discharge at initial pH 5.0, 7.0 and 9.0, the concentration of As(III) was 15.1, 15.3 and 13.9 mg L^{-1}, that of As(V) was 33.6, 33.5 and 48.1 mg L^{-1}, and that of As(T) was 53.1, 44.8 and 61.7 mg L^{-1}, and the corresponding As(T) removal ratio reached 46.9%, 55.2% and 38.3% at initial pH 5.0, 7.0 and 9.0, respectively.

Fig. S11a shows the dissolved Fe^{2+} concentration in As(III) solution at initial pH 5.0 and 9.0 during the charge—discharge processes. With increasing cycle number, the concentration of dissolved Fe^{2+} increased first and reached the maximum of 5.82 and 1.62 mg L^{-1} after 100 cycles, and then decreased to 0.52 and 0.30 mg L^{-1} after 600 cycles at initial pH 5.0 and 9.0, respectively, with the final pH values being 3.8 and 4.2 (Fig. S11b). As indicated by the XRD results, no other mineral was formed on hematite electrode after 600 cycles (Fig. S12). The results of XRD patterns and FTIR spectra indicated that amorphous $FeAsO_4$ was the main product in the precipitate (Fig. S13).

The mass of hematite on the working electrode was increased from 4 to 10 and 15 mg to further enhance the As(III) removal ratio. Fig. 7 shows the concentrations of different As species in As(III) solution (100 mg L^{-1}) during the charge—discharge processes. With increasing cycle number, the concentration of As(III) and As(T) decreased, and that of As(V) increased first and then decreased. With increasing hematite mass from 4.0 to 10 and 15 mg, after 600 cycles of charge—discharge, the concentration of As(III) decreased from 15.3 to 3.4 and 0.1 mg L^{-1}; that of As(V) declined from 33.5 to 19.5 and 1.3 mg L^{-1}; that of As(T) dropped from 44.8 to 22.9 and 1.4 mg L^{-1}; and the

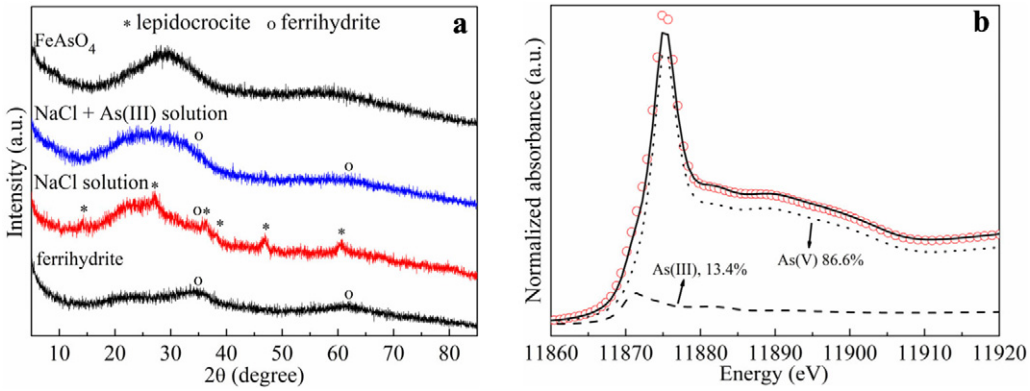

Fig. 5. XRD patterns of the precipitates generated in the mixed solution of 100 mg L^{-1} As(III) and 10 mmol L^{-1} NaCl at initial pH 7.0 after 600 cycles of charge—discharge of the working electrode with 4 mg hematite (a). As K-edge XANES spectra (open circles) and the corresponding linear combination fitting (solid line) of the precipitate generated in the mixed solution (b).

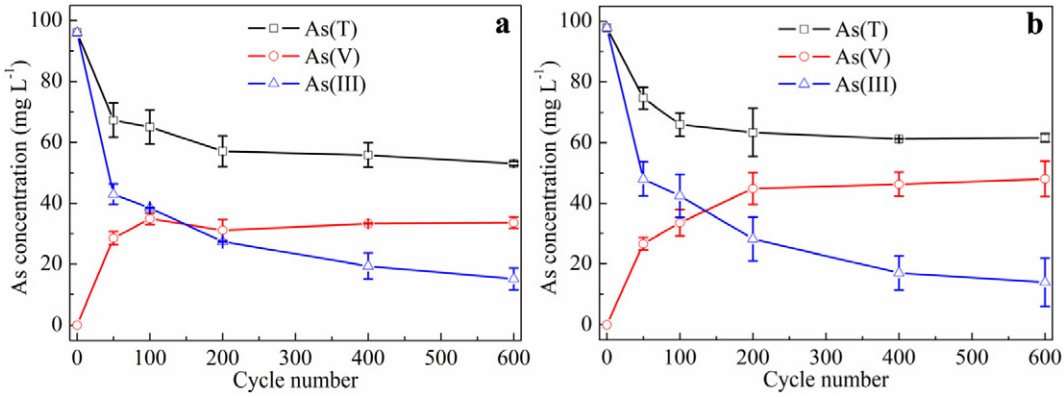

Fig. 6. Concentrations of As(III), As(V) and As(T) in the mixed solution of 100 mg L^{-1} As(III) and 10 mmol L^{-1} NaCl at initial pH 5.0 (a) and 9.0 (b) after different cycles of charge−discharge of the working electrode with 4 mg hematite.

corresponding As(T) removal ratio increased from 55.2% to 76.8% and 98.6%, respectively.

When the hematite mass was controlled at 10 and 15 mg, the concentration of dissolved Fe^{2+} increased first and respectively reached the maximum of 6.5 and 10.1 mg L^{-1} after 100 cycles, and then decreased with increasing cycle number (Fig. S14a). The pH value decreased first and then increased (Fig. S14b). The pH was respectively 5.0 and 5.8 after 600 cycles when the hematite mass was controlled at 10 and 15 mg. After 600 cycles, the XRD and FTIR results of the working electrode and the precipitate formed in the electrochemical systems with 10 and 15 mg hematite were similar to those of the electrochemical system with 4 mg hematite (Figs. S15 and S16).

4. Discussion

The electrochemical removal capacity was significantly higher than the isothermal adsorption capacity (Fig. S2). Additionally, about 8% and 73% of As(T) was removed respectively in the chemical coagulation of As(III) and As(V) (100 mg L^{-1}) using 100 mL $Fe(NO_3)_3$ solution (3.4 mmol L^{-1}) (Fig. S17). These results indicated that the high As(III) removal ratio is due to the electrochemical oxidation and coagulation.

4.1. As(III) oxidation

The oxidation of As(III) to As(V) occurred during the electrochemical removal (Fig. 2). As(III) can be directly oxidized to As(V) on electrode surface in the charge−discharge processes. As reported, the polarized anode facilitated the oxidation of As(III) to As(V) (H_3AsO_3/H_3AsO_4, $E^0 = 0.28$ V, *vs.* SCE) when activated carbon electrode was used for As (III) removal at the cell voltage range of 0.8–1.4 V, and the oxidized As (III) accounted for 50% of the As(T) content at 1.4 V (Dai et al., 2018). In this work, the potential of counter electrode varied within −0.8–1.9 V (*vs.* SCE) in the charge−discharge processes (Fig. S5), which facilitated As(III) oxidation.

OH• and H_2O_2 were formed in the charge−discharge processes (Fig. 3), which can oxidize As(III) (Qiu et al., 2018). In our previous work, H_2O_2 was also formed and contributed to As(III) oxidation during the electrochemical treatment of As(III)-containing wastewater discharged from a mining and smelting plant using birnessite (Liu et al., 2019b). O_2 is easily reduced to H_2O_2 on the electrode due to the low standard electrochemical potential of O_2/H_2O_2 ($E^0 = 0.029$ V, *vs.* SCE) (Feng et al., 2010; Kim et al., 2016; Liu et al., 2019b). In the presence of Fe^{2+}, OH• can be generated from H_2O_2 decomposition due to the catalysis of Fe^{2+} for the Fenton reaction (Brillas et al., 2009). In the microbial fuel cell with γ-FeOOH as the cathode, bio-electro-Fenton was effectively used for As(III) oxidation and removal (Wang et al., 2014). In the presence of benzoic acid or peroxidase in the electrochemical system of 100 mg L^{-1} As(III) and 10 mmol L^{-1} NaCl with initial pH 7.0, no significant change was observed in the concentrations of As species (Fig. 8a and b). These results indicated that the electrochemical reduction of oxygen has no significant effect on As(III) oxidation in this work.

Cl^- can be oxidized to Cl_2 at a high potential due to the standard electrochemical potential of Cl^-/Cl_2 ($E^0 = 1.07$ V, *vs.* SCE), and then ClO^- is generated from Cl_2 hydrolysis (He et al., 2016). ClO^- can be used for As(III) oxidation due to its high oxidation activity (Hu et al., 2012). In the present work, NaCl was used as the background electrolyte, and the potential of the counter electrode varied within −0.8–1.9 V (*vs.* SCE) (Fig. S5). ClO^- was detected in the charge−discharge processes, demonstrating the possible oxidation of As(III) by

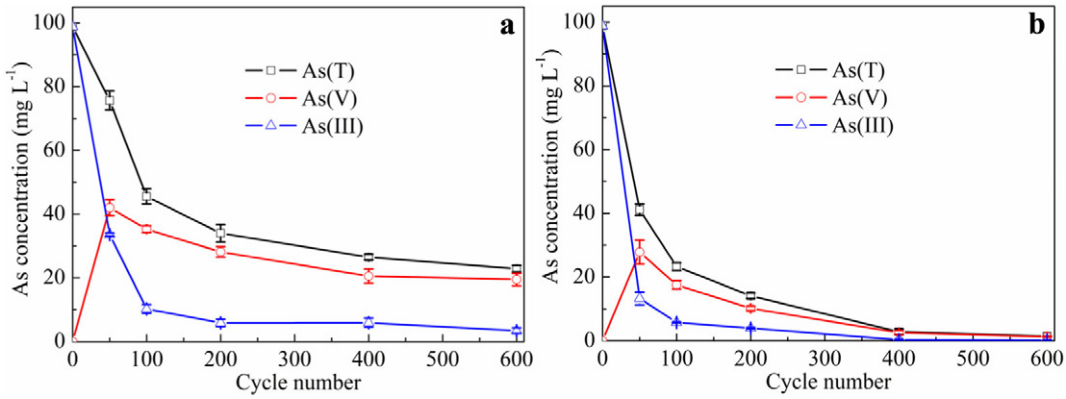

Fig. 7. Concentrations of As(III), As(V) and As(T) in the mixed solution of 100 mg L^{-1} As(III) and 10 mmol L^{-1} NaCl at initial pH 7.0 after 600 cycles of charge−discharge of the working electrode with 10 mg (a) and 15 mg (b) hematite.

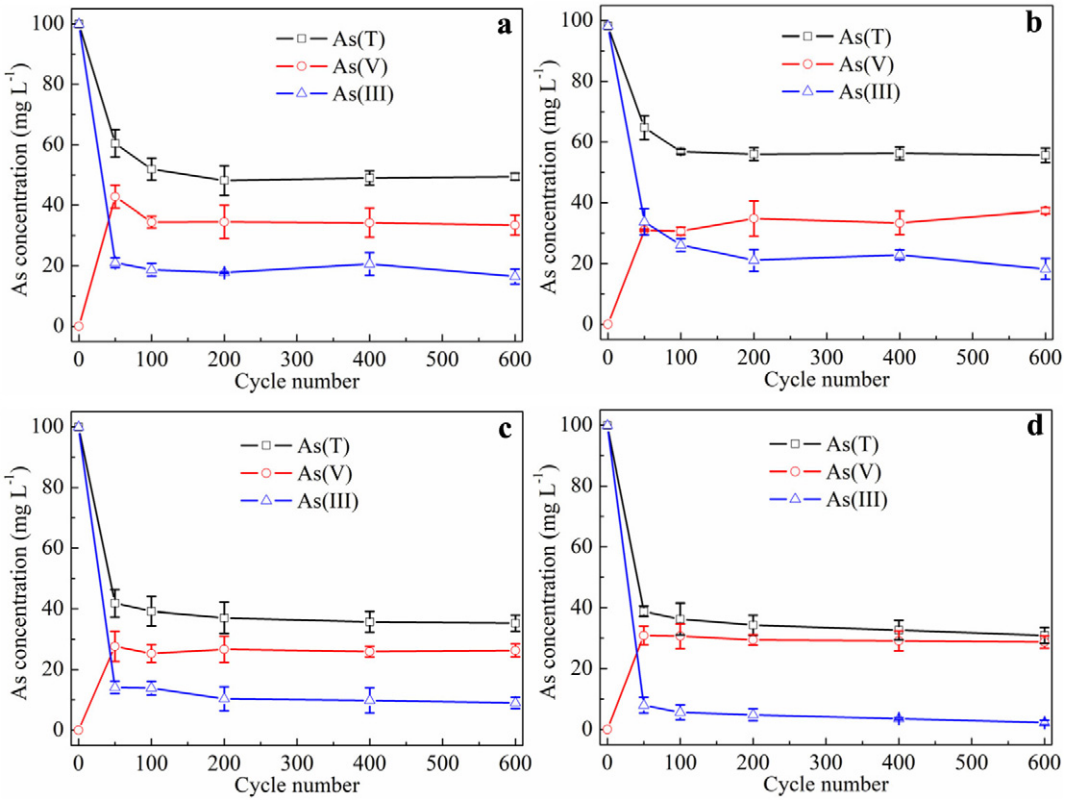

Fig. 8. Concentrations of As(III), As(V) and As(T) in the mixed solution of 100 mg L^{-1} As(III), 10 mmol L^{-1} NaCl and 10 mmol L^{-1} benzoic acid (a)/10 mg L^{-1} peroxidase (b) at initial pH 7.0, and in the mixed solution of 100 mg L^{-1} As(III) and 15 (c)/20 (d) mmol L^{-1} NaCl after different cycles of charge—discharge of the working electrode with 4 mg hematite.

ClO^- (Fig. 3c). In order to further confirm the role of ClO^-, the concentration of NaCl was increased to 15 and 20 mmol L^{-1}. An obvious decrease in As(III) concentration occurred with increasing NaCl concentration (Fig. 8c and d), suggesting that reactive chlorine (ClO^-) possibly contributes much to As(III) oxidation.

4.2. Arsenic removal

The chemical analysis showed that the As content on hematite electrode after charge—discharge accounted for 4.2% of the removed As (T) from the solution. That is to say, 95.8% of the removed As was present in the precipitate. The results of XRD, FTIR and XANES characterization indicated that the removed As mainly existed as $FeAsO_4$ in the precipitate (Fig. 5 and Fig. S9). The formation of $FeAsO_4$ precipitate is one of the key pathways for As removal in electrocoagulation. The further oxidation of Fe^{2+} released from elemental Fe anode by air, ClO^-, reactive oxygen species (ROS), and electrode at high potential would lead to the formation of Fe^{3+}, and ferrihydrite and amorphous iron (hydr)oxides are subsequently generated from the hydrolysis of Fe^{3+} (Nidheesh and Singh, 2017; Tong et al., 2014). The chemical compositions of As-containing iron (hydr)oxides produced from the abiotic oxidation of Fe^{2+} are affected by the As:Fe molar ratio in the presence of As (V) (Song et al., 2015). At initial pH 7.0, the oxidation product of Fe^{2+} changed from the mixture of ferrihydrite, goethite and lepidocrocite to $FeAsO_4$ with increasing As:Fe molar ratio from 0 to 0.11 (Song et al., 2015). In this work, ferrihydrite and lepidocrocite were the main products in the absence of As, which could be ascribed to the presence of Cl^-. The presence of Cl^- could induce the formation of lepidocrocite in Fe^{2+} oxidation by air (Frini and El Maaoui, 1997), which was also observed during the oxidation of $FeCl_2$ solution by the ROS generated from NO_3^- photolysis in our previous work (Liu et al., 2018). In the charge—discharge processes, As(V) was adsorbed on ferrihydrite surface by ligand exchange to form inner-sphere complexes, which would be transformed to $FeAsO_4$ (Jiang et al., 2015).

As reported, Fe^{2+} can react with As(V) to form stable $Fe_3(AsO_4)_2$ in reducing environments, and As(V) will be released from $Fe_3(AsO_4)_2$ to generate $FeAsO_4$ with Fe^{3+} produced from Fe^{2+} oxidation when the potential increases in the reaction system (Doerfelt et al., 2015). A video of the 20th cycle of charge—discharge in As(III) solution (800 mg L^{-1}) at initial pH 7.0 was taken to examine the formation processes of $Fe_3(AsO_4)_2$ (Supporting Video, Video S1). The formation of precipitate was clearly observed around the working electrode in the discharge process. In addition, Fe^{2+} can be rapidly oxidized to Fe^{3+} by H_2O_2 generated from O_2 reduction in the discharge process. Therefore, $FeAsO_4$ rather than $Fe_3(AsO_4)_2$ was produced in As(III) removal.

The possible formation process of amorphous $FeAsO_4$ can be speculated by analyzing the chemical composition and formation stage of precipitate. In the discharge process, As(III) was oxidized by ClO^- and the counter electrode at high potential. The released Fe^{2+} was also oxidized to Fe^{3+} by OH•, H_2O_2 and ClO^- on the surface of the working electrode. Then, As(V) was adsorbed on ferrihydrite surface by ligand exchange to form $FeAsO_4$. In previous studies of the electrocoagulation for As using elemental Fe anode, Fe^{2+} was produced from the oxidation of elemental Fe, and the pH decreased in anodic region ($2H_2O \rightarrow 4H^+ + O_2 + 4e^-$); and O_2 was reduced to H_2O_2 and the pH increased in the cathodic region ($2H_2O + 2e^- \rightarrow H_2 + 2OH^-$) (Song et al., 2017; Tong et al., 2014). In this work, both Fe^{2+} oxidation and As(V) precipitation occurred around the working electrode instead of the electrode surface (Fig. 4). Therefore, the charge—discharge process can be used for *in situ* oxidation and removal of As(III) from aqueous solution.

In traditional electrocoagulation, electrode surface is easily covered by newly formed iron oxide precipitate, which blocks the further release of Fe^{2+} and electron transfer. The passivation of electrode can be alleviated by the replacement of electrodes or periodic polarity reversal of the electrodes (Holt et al., 2005). In this work, the periodic polarity reversal

of electrodes occurred in each charge−discharge process, effectively avoiding the passivation of electrode, which was further demonstrated by the photograph of the working electrode after 600 cycles of charge −discharge in As(III) solution (100 mg L^{-1}) (Fig. S18).

High energy consumption is another challenge for traditional electrocoagulation (Song et al., 2017). In this work, the electrochemical system can be used as a supercapacitor for power output during As(III) removal (Fig. S19). The coulombic efficiency was above 100% in the charge−discharge process, indicating the presence of not fully reversible redox reactions (Liu et al., 2017). In the charge−discharge process of $FeSe_2$ electrode in Na-ion batteries, the collapse of crystal structure resulted in a higher coulombic efficiency than 100% (An et al., 2019). In this work, besides the reduction of hematite and the subsequent release of Fe^{2+} ions, the reduction of O_2, the oxidation of As(III) and the adsorption of As(III,V) contributed much to the higher coulombic efficiency. As a matter of fact, some energy was consumed in the preparation of nanosized hematite and electrode and electrocoagulation operation. The electrochemical system can be used as a supercapacitor in the removal process. Therefore, this electrochemical process can be regarded as energy-efficient.

4.3. Effects of initial pH and hematite mass

With increasing initial pH from 5.0 to 9.0, As(III) concentration changed slightly, indicating that the various As(T) removal ratios could be ascribed to the differences in the adsorption or precipitation amount of As(V) at different initial pH values (Fig. 6). The existing form of iron ions depends on the pH of the reaction solution. Dissolved Fe(II) exists in the form of Fe^{2+} when the pH is below 7.0 (Song et al., 2017). More Fe^{2+} ions were oxidized and precipitated with increasing pH (Liu et al., 2018), leading to a lower Fe^{2+} concentration in the solution and the formation of more iron (hydr)oxides (Fig. S11). Therefore, the As(T) removal ratio increased with increasing initial pH from 5.0 to 7.0. In addition, As(V) adsorption on the iron (hydr)oxides generated in electrocoagulation is also affected by the pH (Song et al., 2017). The point of zero charge (PZC) of ferrihydrite usually varies from 7 to 9 (Zhang et al., 2012). In this work, at initial pH 9.0, the pH rapidly decreased to below 7.0 and the surface of ferrihydrite was positively charged. The increase of initial pH resulted in less positive charge on ferrihydrite surface and a decrease in the adsorption capacity of negatively charged As(V). Therefore, a higher As(T) removal ratio was achieved at initial pH 7.0 than at initial pH 5.0 and 9.0. Generally, the pH of groundwater is close to neutral (Sorg et al., 2014). The pH was determined to be 8.18 for the wastewater discharged from a mining and smelting plant in our previous work (Liu et al., 2019b). Therefore, the charge−discharge technique using hematite has the potential in As removal from real wastewaters.

The mass of active materials on electrode affects the electrochemical performance. The specific capacitance decreased from 1066 to 716 F g^{-1} with the loaded FeOOH mass on the electrode increasing from 1.6 to 9.1 mg cm^{-2} (Owusu et al., 2017). In this work, the electrode area increased with increasing hematite mass (Table S1). The electrochemical specific capacitance of pseudocapacitor depends on the redox reactions of electrode materials and the insertion−desertion or the adsorption −adsorption of ions on electrode surface (Nithya and Arul, 2016). With increasing electrode area and hematite mass, the specific capacitance and coulombic efficiency decreased (Fig. S19), likely due to the relatively low concentrations of background electrolyte and As. At the same current density, less hematite on the electrode could facilitate a better contact between hematite and dissolved As(III) in the solution. The redox reactions of electrode materials mainly occur on the electrode surface in supercapacitor (Pang et al., 2000). The larger electrode area led to the release of more Fe^{2+} ions (Fig. S14), which facilitated As (T) removal. Therefore, although the specific capacitance decreases with increasing hematite mass, a proper increase in electrode area is helpful for the rapid removal of As(III), which provides a reference for the treatment of real As-containing wastewaters.

5. Conclusions

In this work, As(III) can be effectively oxidized and removed from aqueous solution by multi-cycle galvanostatic charge−discharge of the hematite synthesized through a microwave-assisted hydrothermal reaction. The oxidation of As(III) was mainly ascribed to ClO^- and counter electrode at high potential in the charge−discharge processes. As (T) removal can be attributed to As(V) adsorption on ferrihydrite and $FeAsO_4$ formation. The oxidation and precipitation rate of Fe^{2+} and PZC of ferrihydrite lead to the higher As(T) removal ratio at initial pH 7.0 than at initial pH 5.0 and 9.0. The As(T) removal ratio from the As(III) solution increased from 55.2% to 98.6% when the hematite mass on the working electrode was increased from 4 to 15 mg. The passivation of electrode can be alleviated by the periodic redox reaction of hematite electrodes in the charge process. In addition, the energy consumption in As(III) removal can be reduced by power output compared with traditional electrocoagulation. The present work provides a novel strategy for the treatment of As(III)-containing wastewater using iron oxides.

Supplementary data to this article can be found online at https://doi.org/10.1016/j.scitotenv.2019.135678.

Declaration of competing interest

The authors declare that they have no known competing financial interests or personal relationships that could have appeared to influence the work reported in this paper.

Acknowledgements

The study was financially supported by the National Key Research and Development Program of China (Grant Nos. 2017YFD0801000 and 2018YFD0800304), the National Natural Science Foundation of China (Grant Nos. 41571228, 41877025, 41877528 and 41425006) and the Fundamental Research Funds for the Central Universities (Program Nos. 2662018JC055 and 2662017JC025). We are grateful to Dr. Lihong Qin and Dr. Jianbo Cao at Public Laboratory of Electron Microscope of Huazhong Agricultural University for helping with SEM and TEM analyses, and Dr. Lirong Zheng and Dr. Shengqi Chu at Beijing Synchrotron Radiation Facility for the collection of As XANES spectra.

References

An, C., Yuan, Y., Zhang, B., Tang, L., Xiao, B., He, Z., Zheng, J., Lu, J., 2019. Graphene wrapped $FeSe_2$ nano-microspheres with high pseudocapacitive contribution for enhanced Na-ion storage. Adv. Energy Mater. 9, 1900356.

Bindal, S., Singh, C.K., 2019. Predicting groundwater arsenic contamination: regions at risk in highest populated state of India. Water Res. 159, 65–76.

Brillas, E., Sirés, I., Oturan, M.A., 2009. Electro-Fenton process and related electrochemical technologies based on Fenton's reaction chemistry. Chem. Rev. 109, 6570–6631.

Choong, T.S.Y., Chuah, T.G., Robiah, Y., Koay, F.L.G., Azni, I., 2007. Arsenic toxicity, health hazards and removal techniques from water: an overview. Desalination 217, 139–166.

Dai, M., Zhang, M., Xia, L., Li, Y., Liu, Y., Song, S., 2017. Combined electrosorption and chemisorption of As(V) in water by using Fe-rGO@AC electrode. ACS Sustain. Chem. Eng. 5, 6532–6538.

Dai, M., Xia, L., Song, S., Peng, C., Rangel-Mendez, J.R., Cruz-Gaona, R., 2018. Electrosorption of As(III) in aqueous solutions with activated carbon as the electrode. Appl. Surf. Sci. 434, 816–821.

Dhar, R.K., Zheng, Y., Rubenstone, J., van Geen, A., 2004. A rapid colorimetric method for measuring arsenic concentrations in groundwater. Anal. Chim. Acta 526, 203–209.

Doerfelt, C., Feldmann, T., Daenzer, R., Demopoulos, G.P., 2015. Stability of continuously produced Fe(II)/Fe(III)/As(V) co-precipitates under periodic exposure to reducing agents. Chemosphere 138, 239–246.

Donahue, R., Hendry, M.J., 2003. Geochemistry of arsenic in uranium mine mill tailings, Saskatchewan, Canada. Appl. Geochem. 18, 1733–1750.

Feng, C.-H., Li, F.-B., Mai, H.-J., Li, X.-Z., 2010. Bio-electro-Fenton process driven by microbial fuel cell for wastewater treatment. Environ. Sci. Technol. 44, 1875–1880.

Fox, D.I., Stebbins, D.M., Alcantar, N.A., 2016. Combining ferric salt and cactus mucilage for arsenic removal from water. Environ. Sci. Technol. 50, 2507–2513.
Frini, A., El Maaoui, M., 1997. Kinetics of the formation of goethite in the presence of sulfates and chlorides of monovalent cations. J. Colloid Interface Sci. 190, 269–277.
Garg, S., Rong, H., Miller, C.J., Waite, T.D., 2016. Oxidative dissolution of silver nanoparticles by chlorine: Implications to silver nanoparticle fate and toxicity. Environ. Sci. Technol. 50, 3890–3896.
Gude, J.C.J., Rietveld, L.C., van Halem, D., 2017. As(III) oxidation by MnO_2 during groundwater treatment. Water Res. 111, 41–51.
He, D., Wong, C.E., Tang, W., Kovalsky, P., Waite, T.D., 2016. Faradaic reactions in water desalination by batch-mode capacitive deionization. Environ. Sci. Technol. Lett. 3, 222–226.
Holt, P.K., Barton, G.W., Mitchell, C.A., 2005. The future for electrocoagulation as a localised water treatment technology. Chemosphere 59, 355–367.
Hong, J., Liu, L., Luo, Y., Tan, W., Qiu, G., Liu, F., 2018. Photochemical oxidation and dissolution of arsenopyrite in acidic solutions. Geochim. Cosmochim. Acta 239, 173–185.
Hu, C., Liu, H., Chen, G., Jefferson, W.A., Qu, J., 2012. As(III) oxidation by active chlorine and subsequent removal of As(V) by Al_{13} polymer coagulation using a novel dual function reagent. Environ. Sci. Technol. 46, 6776–6782.
Jiang, X., Peng, C., Fu, D., Chen, Z., Shen, L., Li, Q., Ouyang, T., Wang, Y., 2015. Removal of arsenate by ferrihydrite via surface complexation and surface precipitation. Appl. Surf. Sci. 353, 1087–1094.
Jones, A.M., Collins, R.N., Rose, J., Waite, T.D., 2009. The effect of silica and natural organic matter on the Fe(II)-catalysed transformation and reactivity of Fe(III) minerals. Geochim. Cosmochim. Acta 73, 4409–4422.
Joo, S.H., Feitz, A.J., Sedlak, D.L., Waite, T.D., 2005. Quantification of the oxidizing capacity of nanoparticulate zero-valent iron. Environ. Sci. Technol. 39, 1263–1268.
Khan, A.H., Rasul, S.B., Munir, A.K.M., Habibuddowla, M., Alauddin, M., Newaz, S.S., Hussam, A., 2000. Appraisal of a simple arsenic removal method for ground water of Bangladesh. J. Environ. Sci. Health A 35, 1021–1041.
Kim, T., Yu, J., Kim, C., Yoon, J., 2016. Hydrogen peroxide generation in flow-mode capacitive deionization. J. Electroanal. Chem. 776, 101–104.
Liu, L., Luo, Y., Tan, W., Liu, F., Suib, S.L., Zhang, Y., Qiu, G., 2017. Zinc removal from aqueous solution using a deionization pseudocapacitor with a high-performance nanostructured birnessite electrode. Environ. Sci. Nano 4, 811–823.
Liu, L., Jia, Z., Tan, W., Suib, S.L., Ge, L., Qiu, G., Hu, R., 2018. Abiotic photomineralization and transformation of iron oxide nanominerals in aqueous systems. Environ. Sci. Nano 5, 1169–1178.
Liu, L., Peng, Q., Qiu, G., Zhu, J., Tan, W., Liu, C., Zheng, L., Dang, Z., 2019a. Cd^{2+} adsorption performance of tunnel-structured manganese oxides driven by electrochemically controlled redox. Environ. Pollut. 244, 783–791.
Liu, L., Tan, W., Suib, S.L., Qiu, G., Zheng, L., Su, S., 2019b. Enhanced adsorption removal of arsenic from mining wastewater using birnessite under electrochemical redox reactions. Chem. Eng. J. 375, 122051.
Luo, Y., Liu, L., Qiao, W., Liu, F., Zhang, Y., Tan, W., Qiu, G., 2016. Facile crystal-structure-controlled synthesis of iron oxides for adsorbents and anode materials of lithium batteries. Mater. Chem. Phys. 170, 239–245.
Luong, V.T., Kurz, E.E.C., Hellriegel, U., Luu, T.L., Hoinkis, J., Bundschuh, J., 2018. Iron-based subsurface arsenic removal technologies by aeration: a review of the current state and future prospects. Water Res. 133, 110–122.
Nidheesh, P.V., Singh, T.S.A., 2017. Arsenic removal by electrocoagulation process: Recent trends and removal mechanism. Chemosphere 181, 418–432.
Nithya, V.D., Arul, N.S., 2016. Review on α-Fe_2O_3 based negative electrode for high performance supercapacitors. J. Power Sources 327, 297–318.
Nordstrom, D.K., 2002. Worldwide occurrences of arsenic in ground water. Science 296, 2143–2145.
Owusu, K.A., Qu, L., Li, J., Wang, Z., Zhao, K., Yang, C., Hercule, K.M., Lin, C., Shi, C., Wei, Q., Zhou, L., Mai, L., 2017. Low-crystalline iron oxide hydroxide nanoparticle anode for high-performance supercapacitors. Nat. Commun. 8, 14264.
Pang, S.C., Anderson, M.A., Chapman, T.W., 2000. Novel electrode materials for thin-film ultracapacitors: comparison of electrochemical properties of sol-gel-derived and electrodeposited manganese dioxide. J. Electrochem. Soc. 147, 444–450.
Park, J.H., Han, Y.S., Ahn, J.S., 2016. Comparison of arsenic co-precipitation and adsorption by iron minerals and the mechanism of arsenic natural attenuation in a mine stream. Water Res. 106, 295–303.
Peng, Q., Liu, L., Luo, Y., Zhang, Y., Tan, W., Liu, F., Suib, S.L., Qiu, G., 2016. Cadmium removal from aqueous solution by a deionization supercapacitor with a birnessite electrode. ACS Appl. Mater. Interfaces 8, 34405–34413.
Qiao, J.T., Liu, T.X., Wang, X.Q., Li, F.B., Lv, Y.H., Cui, J.H., Zeng, X.D., Yuan, Y.Z., Liu, C.P., 2018. Simultaneous alleviation of cadmium and arsenic accumulation in rice by applying zero-valent iron and biochar to contaminated paddy soils. Chemosphere 195, 260–271.
Qiu, G., Huang, H., Genuino, H., Opembe, N., Stafford, L., Dharmarathna, S., Suib, S.L., 2011. Microwave-assisted hydrothermal synthesis of nanosized α-Fe_2O_3 for catalysts and adsorbents. J. Phys. Chem. C 115, 19626–19631.
Qiu, G., Gao, T., Hong, J., Luo, Y., Liu, L., Tan, W., Liu, F., 2018. Mechanisms of interaction between arsenian pyrite and aqueous arsenite under anoxic and oxic conditions. Geochim. Cosmochim. Acta 228, 205–219.
Shakoor, M.B., Niazi, N.K., Bibi, I., Shahid, M., Saqib, Z.A., Nawaz, M.F., Shaheen, S.M., Wang, H., Tsang, D.C., Bundschuh, J., 2019. Exploring the arsenic removal potential of various biosorbents from water. Environ. Int. 123, 567–579.
Song, J., Jia, S.Y., Yu, B., Wu, S.H., Han, X., 2015. Formation of iron (hydr)oxides during the abiotic oxidation of Fe(II) in the presence of arsenate. J. Hazard. Mater. 294, 70–79.
Song, P., Yang, Z., Zeng, G., Yang, X., Xu, H., Wang, L., Xu, R., Xiong, W., Ahmad, K., 2017. Electrocoagulation treatment of arsenic in wastewaters: a comprehensive review. Chem. Eng. J. 317, 707–725.
Sorg, T.J., Chen, A.S., Wang, L., 2014. Arsenic species in drinking water wells in the USA with high arsenic concentrations. Water Res. 48, 156–169.
Tong, M., Yuan, S., Zhang, P., Liao, P., Alshawabkeh, A.N., Xie, X., Wang, Y., 2014. Electrochemically induced oxidative precipitation of Fe(II) for As(III) oxidation and removal in synthetic groundwater. Environ. Sci. Technol. 48, 5145–5153.
Wang, S., Mulligan, C.N., 2006. Occurrence of arsenic contamination in Canada: sources, behavior and distribution. Sci. Total Environ. 366, 701–721.
Wang, X.Q., Liu, C.P., Yuan, Y., Li, F.B., 2014. Arsenite oxidation and removal driven by a bio-electro-Fenton process under neutral pH conditions. J. Hazard. Mater. 275, 200–209.
Wang, Y., Muramatsu, A., Sugimoto, T., 1998. FTIR analysis of well-defined α-Fe_2O_3 particles. Colloids Surf. A Physicochem. Eng. Asp. 134, 281–297.
Yang, X., Liu, L., Tan, W., Qiu, G., Liu, F., 2018. High-performance Cu^{2+} adsorption of birnessite using electrochemically controlled redox reactions. J. Hazard. Mater. 354, 107–115.
Yang, X., Liu, L., Zhang, M., Tan, W., Qiu, G., Zheng, L., 2019. Improved removal capacity of magnetite for Cr(VI) by electrochemical reduction. J. Hazard. Mater. 26–34.
Zhang, G., Liu, H., Qu, J., Jefferson, W., 2012. Arsenate uptake and arsenite simultaneous sorption and oxidation by Fe-Mn binary oxides: influence of Mn/Fe ratio, pH, Ca^{2+}, and humic acid. J. Colloid Interface Sci. 366, 141–146.